INTERNATIONAL JOURNAL FOR NUMERICAL METHODS IN FLUIDS, VOL. 7, 319–335 (1987)

NUMERICAL SOLUTION OF THE TRANSPORT EQUATION FOR PASSIVE CONTAMINANTS IN THREE-DIMENSIONAL COMPLEX TERRAINS

J. GLEKAS, G. BERGELES AND N. ATHANASSIADIS

Laboratory of Aerodynamics, National Technical University of Athens, Athens, Greece

SUMMARY

This paper presents a numerical solution of the transport equation for heat and species in complex three-dimensional spaces. The solution domain of the equation is transformed into a cube, as also is the governing equation; the resultant equation is solved in the transformed space via a finite difference technique. The validity of the developed computer code is tested by predicting test cases for which either analytical or reliable experimental results exist. Results are also presented for the rate of convergence of the method and the computer storage requirements, from which the validity, the flexibility and the economy of the developed method are proved for flows in real three-dimensional complex terrains.

INTRODUCTION

The effect of topography on the mean wind speed and the structure of the atmosphere adjacent to the ground is of primary importance in cases concerned with the siting of wind generators and tall buildings, the dispersion of air contaminants emitted from stacks, etc.

The development of fast digital computers has made possible the numerical calculation of such geophysical flows, something that complements experimental results. One of the special feature of the numerical methods that have been developed to solve such problems is the way irregular boundaries are modelled, because generally irregular boundaries do not coincide with the co-ordinate lines. There are three alternative ways of tackling this problem.

One method is to lay out a simple mesh (i.e. Cartesian) to cover both the computational space and the boundary; where the boundaries do not coincide with the grid lines, interpolation is used to apply the boundary conditions[1] or the real topography is approximated by a series of blocks (if we use a Cartesian mesh).[2] Such an approach is bound to introduce errors into the solution, because of the inaccurate application of the boundary conditions.

The second alternative is to use an orthogonal grid fitted to the boundaries. This is a very attractive method, but the generation of such a grid in three dimensions is extremely difficult.

The third avenue of approach is the use of a non-orthogonal grid so that the co-ordinate lines coincide with the boundaries. Then a transformation of the co-ordinate system transforms the irregular domain to a unit cube,[3] and the governing equations are solved in the transformed space.[4,5] The disadvantage of this approach is that the equations under the co-ordinate transformation become more complicated than their Cartesian analogues, and as a consequence the computer code becomes more complex. Nevertheless the main advantage of this approach is the regular boundaries, which imply that the boundary conditions can be imposed accurately and

0271–2091/87/040319–17$08.50

Received 30 July 1986

without difficulties. Moreover under the transformation the grid in the computational space can be uniform, whereas in the physical space the grid lines can be gathered to locations of great gradients.

Gal-Chen and Somerville[6,7] adopted this method with the transformed momentum equations written in non-conservative form; however it can be shown[8] that the transformed equations can be written in strong conservation form, and this form of the equations was adopted in the present study.

The present paper proposes a general finite volume algorithm for three-dimensional elliptic flows. The applications that are presented here are concerned with the solution of the temperature (or concentration) equation. First the theoretical background of the model will be presented and then the discretization of the equations. Finally, several preliminary test cases will be presented, followed by the presentation of a practical application which will demonstrate the efficiency of the code.

ANALYTICAL EQUATIONS OF THE MODEL

For general three-dimensional flows, let (x_1, x_2, x_3) be Cartesian co-ordinates, and (X_1, X_2, X_3) generalized curvilinear co-ordinates:

$$X_i = X_i(x_1, x_2, x_3, t), \quad i = 1, 2, 3. \tag{1}$$

Instead of formulating the equations in the curvilinear co-ordinates, by expressing the vector and tensors in the local basis,[9,10] we adopt a different but also general method, which leads to simpler calculations; making a co-ordinate transformation on the Navier–Stokes equations written in the physical space in any convenient co-ordinate system (e.g. Cartesian, spherical), the corresponding equations in the transformed space can be easily obtained in their strong conservation law form.[8]

From the Navier–Stokes equations in Cartesian co-ordinates:

$$\frac{\partial \mathbf{U}}{\partial t} + \frac{\partial \mathbf{F}_i}{\partial x_i} = \frac{\partial \mathbf{R}_i}{\partial x_i}, \tag{2}$$

where the summation convention has been used, the transformed equations can be obtained:

$$\frac{\partial \bar{\mathbf{U}}}{\partial \tau} + \frac{\partial \bar{\mathbf{F}}_i}{\partial X_i} = \frac{\partial \bar{\mathbf{R}}_i}{\partial X_i}, \tag{3}$$

where

$$\mathbf{U} = \begin{bmatrix} \rho \\ \rho u_1 \\ \rho u_2 \\ \rho u_3 \\ \rho E \end{bmatrix}, \quad \mathbf{F}_i = \mathbf{U} u_i + p \begin{bmatrix} 0 \\ \delta_{i1} \\ \delta_{i2} \\ \delta_{i3} \\ u_i \end{bmatrix}, \quad \mathbf{R}_i = \begin{bmatrix} 0 \\ \tau_{i1} \\ \tau_{i2} \\ \tau_{i3} \\ u_j \tau_{ij} - q_i \end{bmatrix}, \tag{4}$$

δ_{ij} is Kronecker's symbol, $E = e + (u_1^2 + u_2^2 + u_3^2)/2$ and

$$\tau_{ij} = \lambda \frac{\partial u_k}{\partial x_k} \delta_{ij} + \mu \left(\frac{\partial u_i}{\partial x_j} + \frac{\partial u_j}{\partial x_i} \right),$$

$$q_i = -(\gamma / Pr) \mu \frac{\partial e}{\partial x_i}.$$

Also

$$\bar{\mathbf{U}} = \mathbf{U} / \mathscr{D}, \quad \bar{\mathbf{F}}_i = \bar{\mathbf{U}} \frac{\partial X_i}{\partial t} + \frac{\mathbf{F}_j}{\mathscr{D}} \frac{\partial X_i}{\partial x_j}, \quad \mathscr{D} = \frac{\partial (X_1, X_2, X_3)}{\partial (x_1, x_2, x_3)},$$

$$\bar{\mathbf{R}}_i = \frac{\mathbf{R}_j}{\mathscr{D}} \frac{\partial X_i}{\partial x_j} \tag{5}$$

and τ_{ij}, q_i are transformed as

$$\tau_{ij} = \lambda \frac{\partial X_l}{\partial x_k} \frac{\partial u_k}{\partial X_l} \delta_{ij} + \left(\frac{\partial X_l}{\partial x_j} \frac{\partial u_i}{\partial X_l} + \frac{\partial X_l}{\partial x_i} \frac{\partial u_i}{\partial X_l} \right) \mu,$$

$$q_i = -(\gamma/Pr)\mu \frac{\partial X_l}{\partial x_i} \frac{\partial e}{\partial X_l}.$$

At this stage we consider the steady-state problem, so we ignore the time derivatives in the above equations. The above equations (3) can be cast in the convenient form

$$\operatorname{div}(\rho \bar{\mathrm{U}} \Phi) = \operatorname{div}(\Gamma_\Phi \operatorname{grad} \Phi) + S_\Phi \tag{6}$$

or

$$\frac{\partial}{\partial X_i} \left[(\rho J) U_i \Phi - (\Gamma_\Phi J^{-1}) \alpha_i \frac{\partial \Phi}{\partial X_i} \right] = S_\Phi, \tag{7}$$

where Φ is any variable u, v, T, $p, \ldots$, etc., $J = \mathscr{D}^{-1}$ is the Jacobian of the transformation, U_i are the contravariant components of the velocity and α_i are parameters depending on the co-ordinate transformation. Confining ourselves to the temperature equation, equation (7) can be written explicitly as

$$\begin{aligned} &\frac{\partial}{\partial X_1} \left[(\rho J) U_1 T - (J^{-1} \Gamma_T)(A^2 + B^2 + C^2) \frac{\partial T}{\partial X_1} \right] \\ &+ \frac{\partial}{\partial X_2} \left[(\rho J) U_2 T - (J^{-1} \Gamma_T)(D^2 + E^2 + F^2) \frac{\partial T}{\partial X_2} \right] \\ &+ \frac{\partial}{\partial X_3} \left[(\rho J) U_3 T - (J^{-1} \Gamma_T)(G^2 + H^2 + I^2) \frac{\partial T}{\partial X_3} \right] = S_T. \end{aligned} \tag{8}$$

The terms $S_T, A, B, \ldots, I$ are defined in Table I.

The velocity field can be obtained, as far as geophysical flows are concerned, from mass consistent models. The next step of the study will be its extension to the whole problem, i.e. to the solution of the flow field (u, v, w velocities) in conjunction with the temperature equation.

DISCRETIZATION OF THE EQUATION

Under the transformation (1), the physical space R (Figure 1), is transformed to the unit cube D in the transformed space. The governing equation (8) is solved in the transformed space where the grid is uniform. The solution domain is divided into volumes such as are shown in Figure 1, and the well known staggered mesh configuration introduced by Harlow and Welch[11] is adopted for the location of the velocities and scalar quantities.

The temperature equation (8) is integrated over the control volume ΔV, obtaining the algebraic equation

$$A_\mathrm{P} T_\mathrm{P} = A_\mathrm{N} T_\mathrm{N} + A_\mathrm{S} T_\mathrm{S} + A_\mathrm{E} T_\mathrm{E} + A_\mathrm{W} T_\mathrm{W} + A_\mathrm{U} T_\mathrm{U} + A_\mathrm{D} T_\mathrm{D} + S_T, \tag{9}$$

where S_T is the source term.

The notations E, W, N, S, U and D stand for the grid nodes surrounding the central grid node P (Figure 1(b)).

Table I

S_T	$\frac{\partial}{\partial x_1}\left\{(J^{-1}\Gamma_T)\left[(FC-AD-BE)\frac{\partial T}{\partial x_2}+(BH-AG-CI)\frac{\partial T}{\partial x_3}\right]\right\}$ $+\frac{\partial}{\partial x_2}\left\{(J^{-1}\Gamma_T)\left[(FC-AD-BE)\frac{\partial T}{\partial x_1}+(DG-EH-FI)\frac{\partial T}{\partial x_3}\right]\right\}$ $+\frac{\partial}{\partial x_3}\left\{(J^{-1}\Gamma_T)\left[(BH-AG-CI)\frac{\partial T}{\partial x_1}+(DG-EH-FI)\frac{\partial T}{\partial x_2}\right]\right\}$
A	$\left\{\frac{\partial x_2}{\partial X_2}\frac{\partial x_3}{\partial X_3}-\frac{\partial x_2}{\partial X_3}\frac{\partial x_3}{\partial X_2}\right\}$
B	$-\left\{\frac{\partial x_3}{\partial X_2}\frac{\partial x_1}{\partial X_3}-\frac{\partial x_3}{\partial X_3}\frac{\partial x_1}{\partial X_2}\right\}$
C	$-\left\{\frac{\partial x_1}{\partial X_2}\frac{\partial x_2}{\partial X_3}-\frac{\partial x_1}{\partial X_3}\frac{\partial x_2}{\partial X_2}\right\}$
D	$-\left\{\frac{\partial x_2}{\partial X_3}\frac{\partial x_3}{\partial X_1}-\frac{\partial x_2}{\partial X_1}\frac{\partial x_3}{\partial X_3}\right\}$
E	$\left\{\frac{\partial x_3}{\partial X_3}\frac{\partial x_1}{\partial X_1}-\frac{\partial x_3}{\partial X_1}\frac{\partial x_1}{\partial X_3}\right\}$
F	$-\left\{\frac{\partial x_1}{\partial X_3}\frac{\partial x_2}{\partial X_1}-\frac{\partial x_1}{\partial X_1}\frac{\partial x_2}{\partial X_3}\right\}$
G	$-\left\{\frac{\partial x_2}{\partial X_1}\frac{\partial x_3}{\partial X_2}-\frac{\partial x_2}{\partial X_2}\frac{\partial x_3}{\partial X_1}\right\}$
H	$-\left\{\frac{\partial x_3}{\partial X_1}\frac{\partial x_1}{\partial X_2}-\frac{\partial x_3}{\partial X_2}\frac{\partial x_1}{\partial X_1}\right\}$
I	$\left\{\frac{\partial x_1}{\partial X_1}\frac{\partial x_2}{\partial X_2}-\frac{\partial x_1}{\partial X_2}\frac{\partial x_2}{\partial X_1}\right\}$

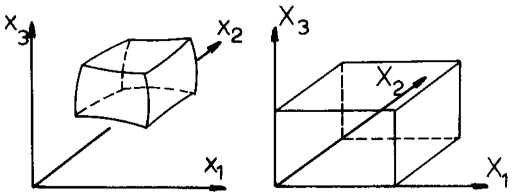

(a)

Figure 1(a). Physical/transformed space

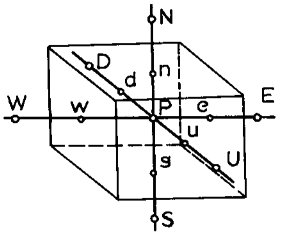

(b)

Figure 1(b). Typical computational cell

The fact that the numerical grid is Cartesian in the solution domain may be masking a problem when imposing Neumann boundary conditions. This problem can be removed either by using a grid that has the grid lines in the physical space normal to the boundaries[12] or by expressing the directional derivatives in the direction normal to the boundaries by the directional derivatives in the grid line directions.[13] It is obvious that, although the latter method needs only trivial calculations to be applied, the former one is more promising. Our intention is to use the former method, but for the application presented here we used the second one.

SOLUTION PROCEDURE

Assuming that the velocity field is known, the algebraic equations (9) are solved with an ADI method, giving the temperature field over the whole domain, under the prescribed boundary conditions.

TEST CASES—VERIFICATION OF THE CODE

Before applying the code to practical applications such as the prediction of the temperature or concentration fields from a point source in the vicinity of a two-dimensional hill, the code was tested in predicting simple flow patterns for which analytical solutions existed.

Test 1—Temperature field from a point source in a uniform parallel flow

In the first test we calculated the diffusion from a point source in a uniform parallel flow. We also considered the special case of pure diffusion from the source where there is no wind blowing.

The main objective of this test was to check the advection and diffusion terms separately.

Figure 2(a) is a definition sketch for this test. The flow was in the X_3 direction, and the grid 11 × 11 × 20, where the 20 grid nodes are in the velocity direction (X_3).

The temperature of the surrounding air was 288 °C and that of the source was 700 °C.

In Figures 2(b) and (c) the temperature distribution at various locations downwind of the source is presented. The temperature distribution is shown at two levels, i.e. (X_2, X_3) and (X_1, X_3), indicating the Gaussian distribution of the temperature far away from the source (Figure 2(d)).

In the case of pure diffusion, where there is no wind, the point source was located at the geometrical centre of the physical space. As was expected, the temperature distribution was symmetrical about the point source.

The results of both the above cases were compared with the results obtained for the same problem from the application of the TEACH code, developed at Imperial College;[14] no difference was apparent between the two sets of results (Figures 2(b), 2(c)).

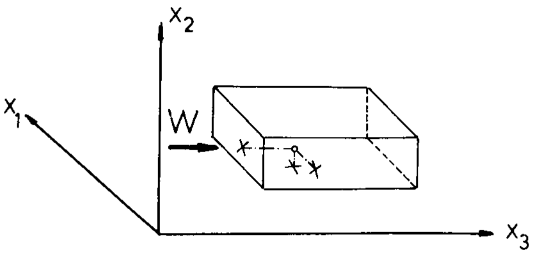

Figure 2(a). Test 1—solution domain

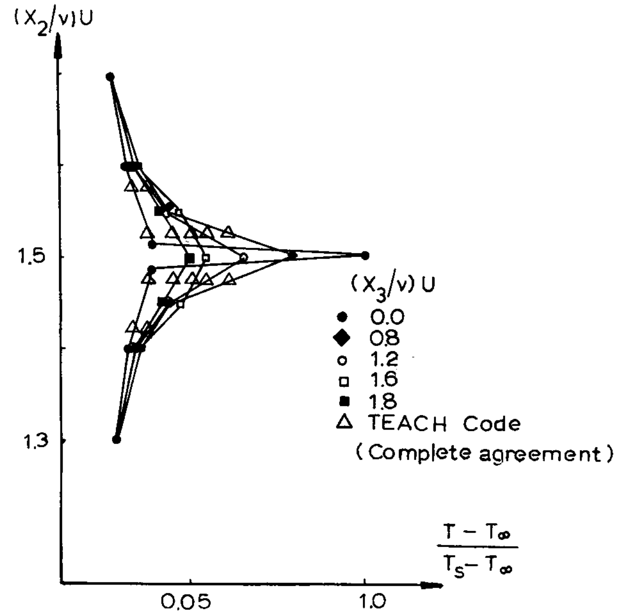

Figure 2(b). Test 1—temperature distribution in (X_2X_3) plane: ● 0·0; ◆ 0·8; ○ 1·2; □ 1·6; ■ 1·8; △ TEACH code (complete agreement)

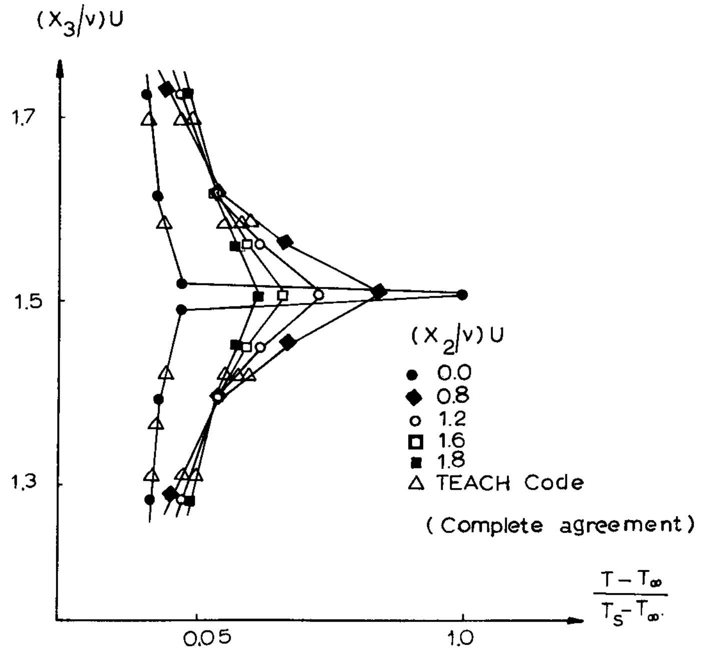

Figure 2(c). Test 1—temperature distribution in (X_1X_3) plane: ● 0·0; ◆ 0·8; ○ 1·2; □ 1·6; ■ 1·8; △ TEACH code (complete agreement)

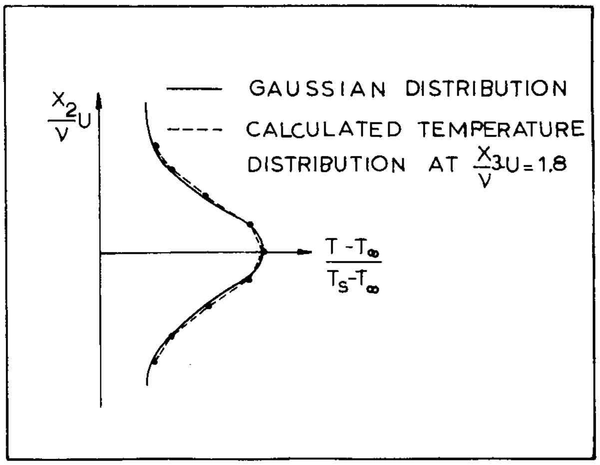

Figure 2(d). Test 1—Gaussian distribution of temperature: ———— Gaussian distribution; ——— calculated temperature distribution at $(x_3/\nu)\ U = 1{\cdot}8$

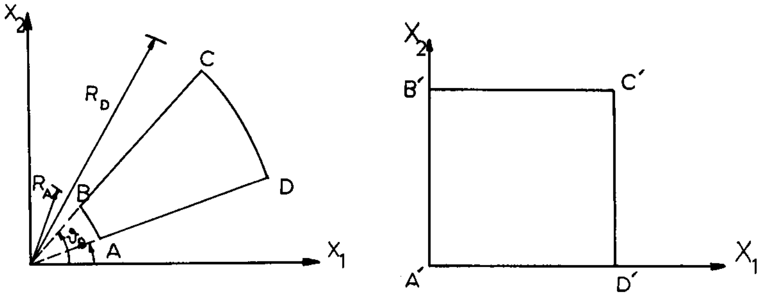

Figure 3. Test 2—physical and transformed spaces

Test 2—Temperature distribution in a convergent two-dimensional channel

In Figure 3, the geometrical configuration of this test is sketched. We considered the two-dimensional motion of a non-viscous fluid in a convergent channel with flat walls.

A sink was located at the origin O and the velocity field was obtained from the equation

$$C = -Q/2\pi r, \tag{10}$$

where Q is the intensity of the source and r the distance from the origin O.

Using the transformation

$$X_1 = \frac{r - r_D}{r_A - r_D}, \quad X_2 = \frac{\vartheta - \vartheta_A}{\vartheta_B - \vartheta_A}, \tag{11}$$

the convergent channel was transformed to a unit square $(0 \leqslant X_1 \leqslant 1, 0 \leqslant X_2 \leqslant 1)$.

Along the line CD $(r = r_D$ and $\vartheta = \vartheta_A - \vartheta_B)$, we imposed a linear temperature variation $(T_A = 300\,^\circ\mathrm{C}, T_B = 400\,^\circ\mathrm{C})$, and selecting the Peclet number Pe (representing convection/diffusion) to be much greater than 1 $(Pe \gg 1)$, we calculated the temperature distribution in the convergent channel. The lines of equal temperature coincided with the streamlines.

Test 3—mass and temperature source in parallel flow

The third test considered the two-dimensional case of a mass source in a parallel flow.[15] Together with the mass source, a temperature source was located at the same point. Selecting the Peclet number to be much greater than 1, we calculated the temperature distribution. As before (test 2), the lines of equal temperature represent the streamlines, because the diffusion term is negligible compared with the convection term.

In Figure 4(a), the geometrical configuration of the test is sketched. The grid was 15 × 15.

From the calculated temperature distribution, the temperature gradient was obtained and compared with the velocity gradient. The comparison is shown in Figure 4(b). The differences between the temperature and velocity gradients were very small and are attributed to the coarseness of the numerical grid.

Test 4—parallel flow past a sphere (very slow motion)

The fourth test considered the temperature distribution in the vicinity of a sphere placed in parallel flow with Reynolds number $Re \ll 1$. This is a case of creeping motion, and the oldest solution for the velocity field was given by Stokes.[16]

In Figure 5, the physical and transformed spaces are sketched. The transformation of the co-ordinates is

$$[0 \leqslant X_1 \leqslant 1], \quad X_1 = \frac{r - r_1}{r_2 - r_1} = \frac{(x_1^2 + x_2^2 + x_3^2)^{1/2} - r_1}{r_2 - r_1},$$

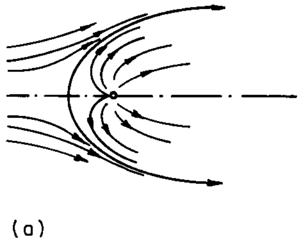

Figure 4(a). Test 3—flow field sketch

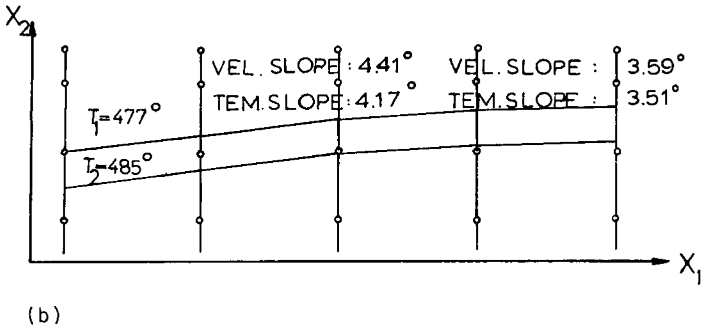

Figure 4(b). Test 3—lines of constant temperature

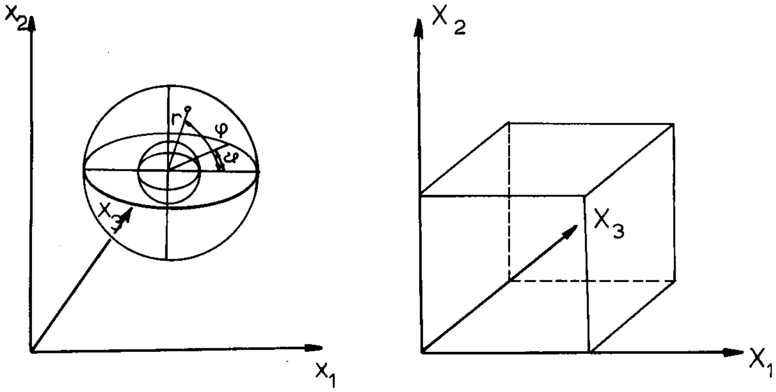

Figure 5. Test 4—physical and transformed spaces

$$[0 \leqslant X_2 \leqslant 1], \quad X_2 = \frac{\varphi - \varphi_3}{\varphi_4 - \varphi_3} = \frac{\arctan[x_2/(x_1^2 + x_3^2)^{1/2}] - \varphi_3}{\varphi_4 - \varphi_3}, \tag{12}$$

$$[0 \leqslant X_3 \leqslant 1], \quad X_3 = \frac{\vartheta - \vartheta_3}{\vartheta_4 - \vartheta_3} = \frac{\arctan(x_3/x_1) - \vartheta_3}{\vartheta_4 - \vartheta_3}.$$

The flow is parallel in the x_3 direction; then the distributions of the Cartesian components of the velocity, u, v and w, and of the pressure, are given by the equations

$$u = U_\infty \frac{3}{4} \frac{R x_1 x_3}{r^3} \left(\frac{R^2}{r^2} - 1 \right), \tag{13}$$

$$v = U_\infty \frac{3}{4} \frac{R x_2 x_3}{r^3} \left(\frac{R^2}{r^2} - 1 \right), \tag{14}$$

$$w = U_\infty \frac{3}{4} \frac{R x_3^2}{r^3} \left(\frac{R^2}{r^2} - 1 \right) - \frac{1}{4} \frac{R}{r} \left(3 + \frac{R^2}{r^2} \right) + 1, \tag{15}$$

$$p - p_\infty = -\frac{3}{2} \frac{\mu U_\infty R x_3}{r^3}. \tag{16}$$

An important characteristic of the creeping motion is that the pressure field satisfies the potential equation

$$\operatorname{div} \operatorname{grad}(p) = \Delta(p) = 0, \tag{17}$$

an equation which is satisfied by the temperature too.

Thus, the fourth test is concerned with the temperature distribution in the vicinity of the sphere, when the temperature distribution on the sphere is identical to that of the pressure, i.e.

$$T - T_\infty = -\frac{3}{2} \frac{\Gamma_T U_\infty x_3}{R^2}. \tag{18}$$

The Reynolds number was 0·14. The calculated temperature distribution was compared with the analytical solution, given by the equation

$$T - T_\infty = -\frac{3}{2} \frac{\Gamma_T U_\infty R x_3}{r^3}. \tag{19}$$

In Figure 6(a) the temperature distribution around the sphere is presented, for three different numerical grids. In Table II the differences between the analytical solution and the computed values are given for the three grids. It is obvious that near the sphere, where the temperature gradients are very steep, the finest grid (30 x 7 x 13 nodes), gives the better results, in close agreement to the analytical solution (error less than 1 per cent). In Figure 6(b) the rates of convergence for the three different grids are presented. It is apparent that for the finest grid (30 x 7 x 13 nodes), the number of iterations was increased compared with that for the coarser grids.

For the same geometrical configuration, the case of pure diffusion was also considered. The temperature of the sphere was taken as 100 °C, and the temperature at the outer boundary of the physical space (which was located 10 radii of the sphere away from the sphere), was taken as 20 °C.

In Figure 7 the computed temperature distribution is compared with the analytical solution ($T = -C_1(1/r) + C_2$, where the constants C_1 and C_2 are obtained from the boundary conditions, i.e. for $r = r_1, T = T_1$ and for $r = r_2, T = T_2$), for the three different grids. Again, near the sphere where the temperature gradients are steep, the finest grid (30 x 7 x 13 nodes), gave the better results (error less than 0·5 per cent).

PRACTICAL APPLICATION

The algorithm was used to calculate the concentration field from a point source in a hilly terrain, and the results were compared with the experimental data of the Joint Soviet–American hill study programme of the Environmental Protection Agency at RTP.[17]

The velocity field which was used as input to our code was from the experimental data, and the results concerned different stack heights and source locations, relative to the hill. The hill shape was two-dimensional (Figure 8), with the following parametric equations:

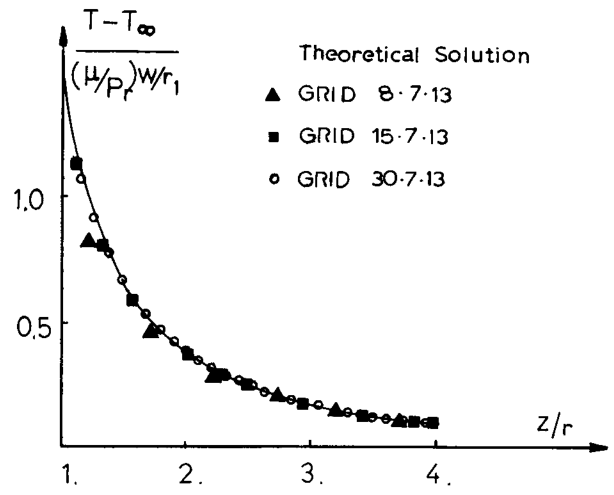

Figure 6(a). Test 4—temperature distribution around a sphere in parallel uniform flow: ——— theoretical solution; ▲ grid 8 x 7 x 13; ■ grid 15 x 7 x 13; ○ grid 30 x 7 x 13

Table II

x_3	$(T-T_\infty)R/(\mu/Pr)U_\infty$	Calculated
1·000	−1·500	−1·500
1·054	−1·350	−1·310
1·161	−1·113	−1·099
1·268	−0·933	−0·927
1·375	−0·794	−0·789
1·482	−0·683	−0·680
1·590	−0·594	−0·586
1·697	−0·521	−0·520
1·804	−0·461	−0·458
1·911	−0·411	−0·410
2·018	−0·368	−0·365
2·125	−0·332	−0·330
2·230	−0·300	−0·297
2·340	−0·274	−0·271
2·446	−0·251	−0·251
2·554	−0·230	−0·229
2·660	−0·212	−0·212
2·767	−0·196	−0·195
2·875	−0·182	−0·180
2·982	−0·169	−0·168
3·089	−0·157	−0·157
3·196	−0·147	−0·146
3·304	−0·137	−0·137
3·410	−0·129	−0·129
3·510	−0·122	−0·122
3·625	−0·114	−0·114
3·730	−0·108	−0·108
3·840	−0·102	−0·102
3·950	−0·096	−0·096
4·000	−0·094	−0·094

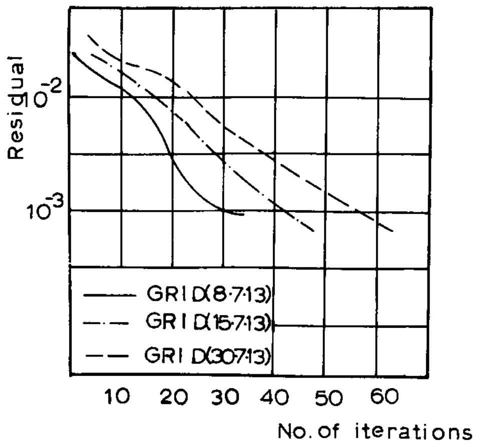

Figure 6(b). Test 4—convergence rates for the three grids

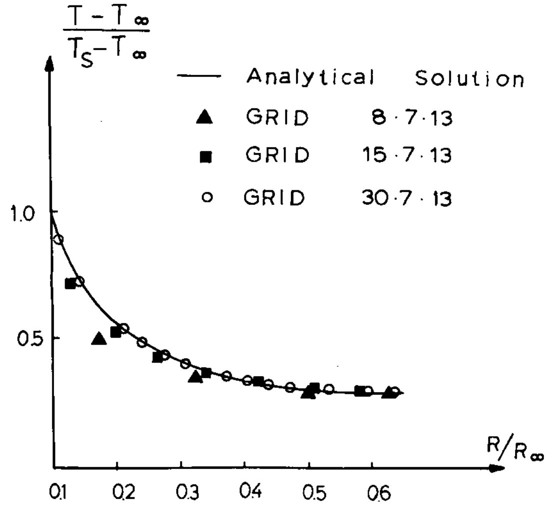

Figure 7. Diffusion/temperature distribution: ——— analytical solution; ▲ grid 8 × 7 × 13; ● grid 15 × 7 × 13; ○ grid 30 × 7 × 13

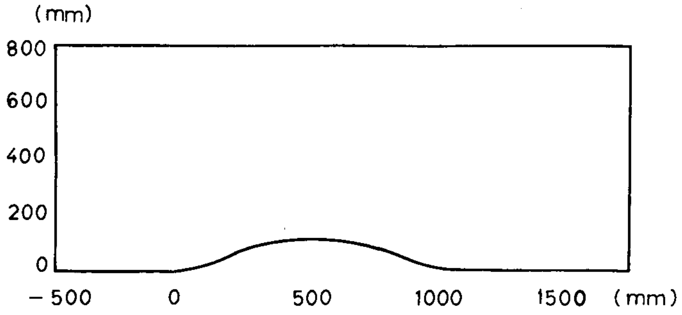

Figure 8. The RTP two-dimensional hill

if $|\xi| < a$

$$x_1 = \tfrac{1}{2}\xi\left\{1 + \frac{a^2}{\xi^2 + m^2(a^2 - \xi^2)}\right\},$$
$$x_2 = \tfrac{1}{2}m\sqrt{(a^2 - \xi^2)}\left\{1 - \frac{a^2}{\xi^2 + m^2(a^2 - \xi^2)}\right\}, \tag{20}$$

if $|\xi| > a$

$$x_1 = \tfrac{1}{2}\mathrm{sign}(\xi)\{|\xi| + m\sqrt{(\xi^2 - a^2)} + a^2[|\xi| + m\sqrt{(\xi^2 - a^2)}]^{-1}\}, \tag{21}$$
$$x_2 = 0,$$

where $m = (h_0/a) + \sqrt{[(h_0/a^2 + 1]}$, h_0 is the height of the hill, a is the half-width of the hill, ξ is an arbitrary parameter, x_1 is directed along the approaching flow direction and x_2 is directed vertically upwards.

The applied co-ordinate transformation was

$$X_1 = \frac{x_1}{L}, \quad 0 \leqslant X_1 \leqslant 1,$$

$$X_2 = \frac{x_2 - s(x_1)}{H - s(x_1)}, \quad 0 \leqslant X_2 \leqslant 1, \tag{22}$$

where L is the maximum distance in the x_1 direction, $s(x_1)$ is the ground elevation (a function of x_1) and H is the vertical height of the physical space, (Figure 9).

For calculating pollutant concentrations using the solution of the diffusion equation in its parabolic form, it is neccessary to determine the vertical diffusivity K_y (as well as the lateral diffusivity K_z in the case of three-dimensional motion). We assume that the diffusion in the streamwise direction is negligible compared to advection.

The vertical diffusivity was calculated from the relations suggested by Berlyand and Genikhovich:[18]

$$\begin{aligned} K_y &= kU_*(x_2 + z_0), \quad \text{when} \quad x_2 - s(x_1) < h, \\ K_y &= kU_*(h + z_0), \quad \text{when} \quad x_2 - s(x_1) \geqslant h, \end{aligned} \tag{23}$$

where U_* is the friction velocity, z_0 is the roughness length, h is the surface layer height and k is von Karman's constant ($= 0{\cdot}4$).

Values of U_*, z_0 and h were determined in accordance with wind tunnel measurements.[18]

For the boundary condition on the ground (i.e. $K_y(\partial C/\partial \bar{n}) = 0$), special care was taken for the normal derivative $\partial C/\partial \bar{n}$ because the co-ordinate lines x_1 and x_2 are not orthogonal. The normal derivative can be expressed in terms of directional derivatives

$$\frac{\partial C}{\partial \bar{n}^{(X_1)}} = \frac{\partial C}{\partial X_2} - \frac{\dfrac{\partial s(x_1)}{\partial x_1}}{L + \dfrac{\partial s(x_1)}{\partial x_1}} \frac{\partial C}{\partial X_1}, \tag{24}$$

where $s(x_1)$ is the ground elevation, C is the concentration and $\bar{n}^{(X_1)}$ is the normal to the X_1 co-ordinate line.

The grid was 17 × 20, with 17 nodes in the x_1 direction and with 20 nodes in the x_2 direction.

The code was tested for a hill with aspect ratio $n = (a/h_0) = 8$ (smooth hill, with maximum slope 10 °), and for stacks located at the upwind base, the top and the downwind base of the hill, and for three different stack heights, i.e. $H_s = h_0/4, h_0/2, h_0$.

The results for the values and positions of maximum surface concentrations, were compared with the experimental data, as well as with the calculations of two numerical models (QPM and WMDM models) used in Reference 18 (Figures 10–14).

Figure 10 shows that the surface concentrations predicted by the present method, when the stack is located upwind of the hill, are very close to the measured values, as well as to the predictions of the QPM model used in Reference 18.

The same conclusion is apparent from Figure 11, where the stack is located at the top of the hill;

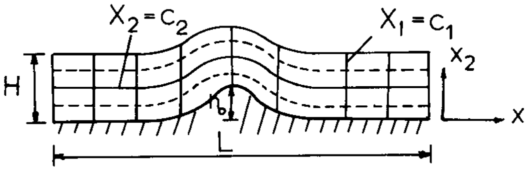

Figure 9. Numerical grid in the physical space

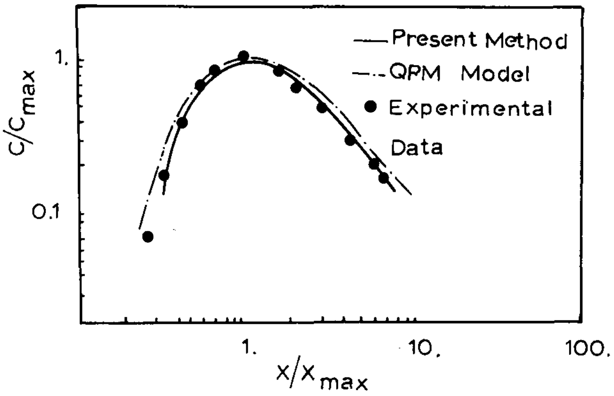

Figure 10. Comparison of surface concentrations predicted by QPM, the present method and experimental data; hill 8; $H_s = h_0/2$; upwind base stack location

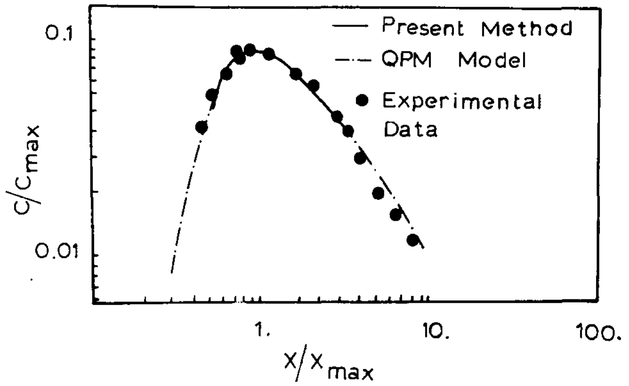

Figure 11. Comparison of surface concentrations predicted by QPM, the present method and the experimental data; hill 8; $H_s = h_0/2$; top of the hill stack location

the results of the present method are, however, in slightly better agreement with the experimental data than the results of the QPM model.

Figure 12 shows that the calculated position and value of maximum concentration is very close to the measured one, for the three stack heights ($h_0/4, h_0/2, h_0$). Comparing the results with those of the WMDM numerical model, the present method gives much better results for stack height $H_s = h_0/4$, whereas for $H_s = h_0/2$ and h_0 the two codes give similar results.

In Figure 13 surface concentrations predicted by the QPM model, the present method and experimental data, are compared. The stack is located downwind of the hill. Again the present method gives results closer to the experimental data than the QPM model.

Figure 14 shows again that when the source is located at the downwind base of the hill, the present results are very close to the experimental results, whereas the WMDM code is not, specially for $H_s = h_0/4$ and $H_s = h_0/2$.

In Figure 15 is presented the rate of convergence of the code, for the various cases to which it was applied. The case when the stack is located downwind of the hill has the highest rate of convergence; this is due to the parabolicity of the species field.

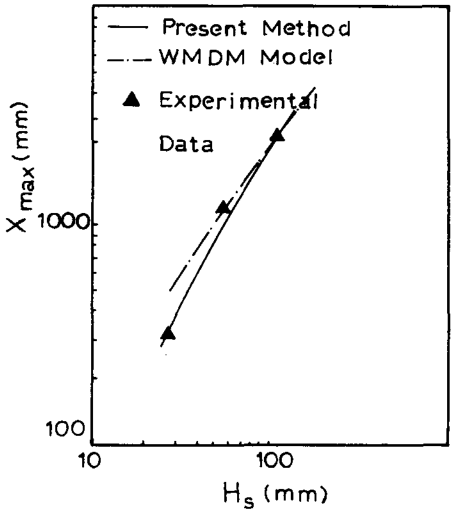

Figure 12. Comparison of distances to location of maximum surface concentration predicted by WMDM, the present method and experimental data; hill 8; top of the hill stack location

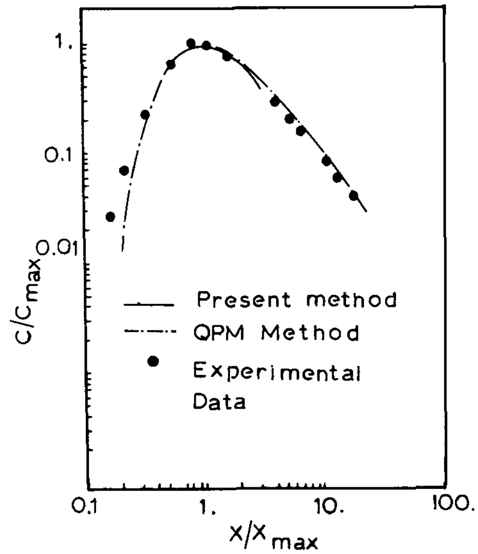

Figure 13. Comparison of surface concentrations predicted by QPM, the present method and experimental data; hill 8; $H_s = h_0/2$; downwind stack location

CONCLUSIONS

The present paper has presented the basic features of a method for solving three-dimensional elliptic flow equations. The main feature of the method is its capability to work without difficulty with complicated geometries, because the method transforms the complex physical space to a unit cube, in which the governing equations are solved.

In this paper applications which were concerned with the energy and concentration equations have been presented.

The velocity field was taken either from analytical relations (where they were available) or from

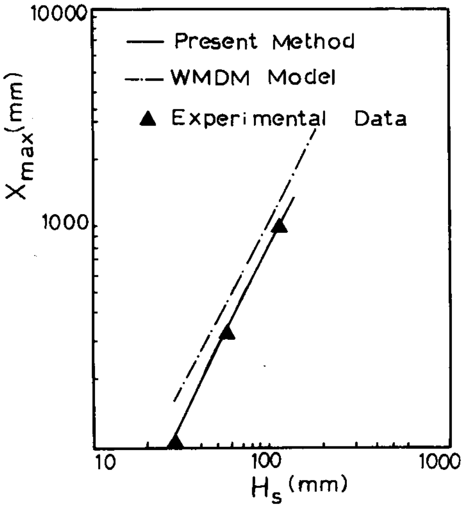

Figure 14. Comparison of distances to location of maximum surface concentration predicted by WMDM, the present method and experimental data; hill 8; downwind base stack location

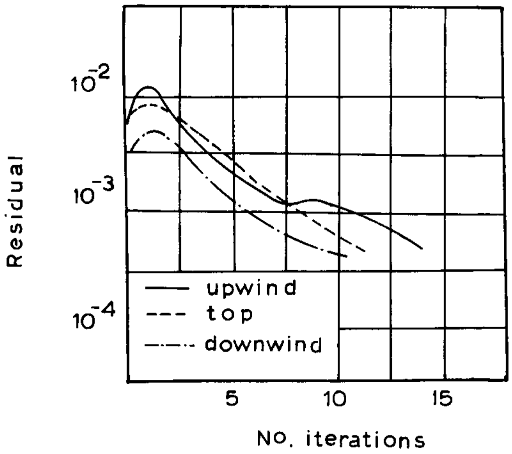

Figure 15. Convergence rates for the three cases considered

experimental data. In all the cases to which the method was applied, the results were close to the analytical solutions or the experimental data, something that demonstrates the reliability of the code.

The next step will be the extension of the code to solve the momentum equations in conjunction with the energy/concentration solver.

NOMENCLATURE

a	Half-width of the hill
$A,\ldots,I$	Transformation coefficients
e	internal energy
h_0	Height of the hill
h	Surface layer height
J	Jacobian of the transformation
k	von Karman's constant

K_y	Vertical diffusivity
p	pressure
Pe	Peclet number
Pr	Prandtl number
Q	Intensity of the point source
$s(x_1)$	Ground elevation
u_i	Cartesian components of the velocity
U_i	Contravariant components of the velocity
U_*	Friction velocity
x_i	Cartesian co-ordinates
X_i	Generalized curvilinear co-ordinates
z_0	Roughness length
α_i	Transformation parameters
γ	ideal gas gamma
Γ_Φ	Diffusion coefficient for variable Φ
λ	coefficient of viscous traction
μ	Molecular viscosity
ν	Kinematic viscosity
ξ	Arbitrary parameter
τ_{ij}	Stress tensor
$\mathscr{D}$	J^{-1}

REFERENCES

1. P. J. Mason and R. I. Sykes, 'Three dimensional numerical integrations of the Navier–Stokes equations for flow over surface-mounted obstacles', *J. Fluid Mech.*, **91,** 433–450 (1979).
2. C. W. Hirt and J. L. Cook, 'Calculating 3-D flows around structures and over rough terrain', *J. Comp. Phys.*, **10,** 324–340 (1972).
3. N. Phillips, 'A coordinate system having some special advantages for numerical forecasting', *J. Meteorology*, **14,** 184–185 (1957).
4. C. R. Maliska, G. D. Raithby, 'A method for computing three-dimensional flows, using non-orthogonal boundary fitted co-ordinates', *Int. j. numer. methods fluids*, **4,** 519–537 (1984).
5. Joseph L. Steger, 'Implicit finite-difference simulation of flow about arbitrary 2D geometries', *AIAA Journal*, **16** (7), 679–686 (1978).
6. Tzvi Gal-Ghen and Richard Somerville, 'Numerical solution of the Navier–Stokes equations with topography', *J. Comp. Physics*, **17,** 276–310 (1975).
7. Tzvi Gal-Ghen and Richard Somerville, 'On the use of a coordinate transformation for the solution of the Navier–Stokes equations', *J. Comp. Physics*, **17,** 209–228 (1975).
8. H. Viviand, 'Formes conservatives des equations de la dynamique des gaz', *La Rech. Aerosp.*, no. 1974-1, 65-66 (1974).
9. H. Hollanders and V. Viviand, 'The numerical treatment of compressible high Reynolds number flows', *VKI Lecture Series*, 1979–6.
10. Z. Warsi, K. Devarayaly and J. F. Thompson, 'Numerical solution of the Navier–Stokes equations for arbitrary blunt bodies in supersonic flows', *Numerical Heat Transfer*, **1,** (4), 499–516 (1978).
11. F. H. Harlow and J. E. Welch, 'Numerical calculation of time dependent viscous incompressible flow of fluid with free surface', *Phys. Fluids*, **8,** (12), 2182–2189 (1965).
12. C. F. Shieh, 'Three-dimensional grid generation using elliptic equations with direct grid distribution control', *AIAA Journal*, **22** (3), 361–364 (1984).
13. J. F. Thompson, F. Thames and W. Mastin, 'Aerodynamic analyses requiring advanced computers', Langley Research Center, 1975.
14. S. V. Patankar and D. B. Spalding, 'A calculation procedure for heat, mass and momentum transfer in three-dimensional parabolic flows', *Int. J. Heat Mass Transfer*, **15,** 1787–1806 (1972).
15. G. K. Batchelor, *An Introduction to Fluid Dynamics*, Cambridge University Press, 1980.
16. H. Schlichting, *Boundary Layer Theory*, 1978, p. 112.
17. L. H. Khurshudyan, W. H. Snyder and I. V. Nekrasov, 'Flow and dispersion of pollutants over two-dimensional hills', *Summary Report of Joint Soviet–American Study, EPA-600/4-81-067*, August 1981.
18. M. E. Berlyand and E. L. Genikhovich, 'Atmospheric diffusion and the structure of the air flow above an inhomogeneous surface', *Proc. Inter. Symp. on Meteorol. Aspects of Air Pollut.*, Leningrad, 1968; Hydromet Press, Leningrad, USSR, 1971.